Available online at www.sciencedirect.com
ScienceDirect
Trans. Nonferrous Met. Soc. China 35(2025) 1907−1918
Transactions of Nonferrous Metals Society of China
www.tnmsc.cn

Isothermal and cyclic oxidation behaviour of Ni−25Cr−10Al−0.5Y coating deposited by AIP and magnetron sputtering at 1323 K

Chun-tang YU[1], Shu-tao CHEN[1], Xiao-yun LI[1], Wen-yao SUN[2], Min FENG[3,4], Cheng-yang JIANG[5], Wan-qi PU[1], Han-qing XIE[1], De-quan WU[6], Sheng-long ZHU[7], Fu-hui WANG[8]

1. School of Materials Science and Engineering, Chongqing University of Technology, Chongqing 401320, China;
2. Yantai Research Institute, Harbin Engineering University, Yantai 264000, China;
3. School of Chemistry and Materials Science, Hangzhou Institute for Advanced Study, University of Chinese Academy of Sciences, Hangzhou 310024, China;
4. State Key Laboratory of High Performance Ceramics and Superfine Microstructure, Shanghai Institute of Ceramics, Chinese Academy of Sciences, Shanghai 200050, China;
5. Zhongfa Aviation Institute of Beihang University, Hangzhou 310023, China;
6. Southwest Institute of Technology and Engineering, Chongqing 400039, China;
7. Shi-Changxu Innovation Center for Advanced Materials, Institute of Metal Research, Chinese Academy of Sciences, Shenyang 110016, China;
8. Shenyang National Laboratory for Materials Science, Northeastern University, Shenyang 110819, China

Received 12 October 2023; accepted 11 May 2024

Abstract: Two kinds of NiCrAlY coatings (Ni−25Cr−10Al−0.5Y) were prepared on K417 superalloy using ion plating (AIP) and magnetron sputtering (MS), respectively. The isothermal and cyclic oxidation behaviors of the two NiCrAlY coatings were evaluated at 1323 K in stair air. The results revealed that the nanocrystalline NiCrAlY coating exhibited better isothermal and cyclic oxidation resistance compared to the conventional NiCrAlY at 1323 K. The mass gain and parabolic rate constant K_p of the nanocrystalline NiCrAlY coating were 45.2% and 44.7% lower than those of the conventional NiCrAlY coating, respectively. During cyclic oxidation, the tendency for spallation of the oxide scale was evidently decreased by nanocrystallization due to the formation of a continuous, compact, adherent, and slow-growing exclusive α-Al_2O_3 scale. The mechanism responsible for the improvement of the nanocrystalline NiCrAlY coating was discussed.

Key words: MCrAlY; nanocrystalline; thermal grown oxide; high-temperature oxidation; spallation

1 Introduction

Driven by the continuous demands for less emission and higher power out efficiency, advanced thermal barrier coatings (TBCs) are applied to the hot components of gas turbines to increase the inlet gas temperature [1−3]. TBCs are usually composed of two layers: the ceramic top coat (TC) composed of yttria-partially-stabilized zirconia (YSZ) providing thermal insulation, and the metallic bond coat (BC) usually made of MCrAlY (M=Ni and/or Co) and Pt-modified aluminide coatings. A thermally grown oxide (TGO) will inevitably form at the TC/BC interface during high-temperature exposure [4−7]. It is widely accepted that the formation and growth of TGO during service is one of the most vital issues responsible for the TBCs

Corresponding author: Wen-yao SUN, Tel: +86-17824032549, E-mail: sunwenyao@mail.neu.edu.cn;
Min FENG, Tel: +86-18840041506, E-mail: fengmin@ucas.ac.cn
https://doi.org/10.1016/S1003-6326(25)66790-2

failure [8−10]. An ideal TGO should be continuous, compact, adherent, and slow-growing oxide scale, which has excellent resistance to elevated temperatures and hot corrosion [11−13]. The exclusive α-Al_2O_3 scale is considered as the most desirable oxide scale, due to its stable nature and low growth rate [14−17].

MCrAlY has a good balance of high-temperature oxidation and hot corrosion resistance [12−14]. During thermal exposure, however, the effective component (Al element) in the coating will be consumed out rapidly due to the formation of the oxide scale and elemental interdiffusion between the coating and the substrate. Non-protective oxides, such as spinel with a loose porous structure and fast growth rate, will then form on the surface, leading to the premature failure of TBCs [18−20]. Therefore, the way to inhibit the formation of detrimental spinel phases and improve the high-temperature oxidation resistance has attracted the attention of many researchers. Nanocrystalline coating with columnar nanosized grains can favor the outward diffusion of Al element and the release of thermal stress, which results in high resistance to oxidation and scale spallation [16−18].

In our current work, a nanocrystalline NiCrAlY coating was deposited on K417 superalloy by magnetron sputtering. The isothermal and cyclic oxidation behavior of nanocrystalline NiCrAlY coating was investigated at 1050 °C in static air compared with the conventional NiCrAlY coating prepared by arc ion plating (AIP). The effect of nanocrystalline structure on high-temperature oxidation behavior of the NiCrAlY coating was intensively discussed. Although there is some literature available on the effect of nanocrystalline structure on the high-temperature oxidation behavior of NiCrAlY coating, previous research in this area is not very systematic. The innovation of the current study lies in the systematic comparison of the isothermal and cyclic oxidation behavior of the nanocrystalline NiCrAlY coating with that of the conventional one, which can guide the design of coatings in the future.

2 Experimental

2.1 Preparation of materials and coatings

Ni-based superalloy K417 was used as the substrate material, with the following nominal composition: Co 9.5−14.0; Cr 8.5−9.5; Al 4.8−5.7; Ti 4.5−5.0; Mo 2.5−3.5; V 0.6−0.9, minor C, Fe less than 1.0, Ni in balance, wt.%. Cylindrical specimens of 2 mm in thickness and 15 mm in diameter were machined using a spark discharge machine. Subsequently, specimens were ground down to a 400-grit surface finish and humidly blasted with 300 mesh alumina grits. The samples were degreased by boiling in a 30 g/L NaOH solution, followed by ultrasonic cleaning in ethanol for 20 min. After that, a NiCrAlY layer with a thickness of 30 μm was deposited onto the prepared samples by a high-vacuum AIP machine (DH−15, Beiyu Vacuum Technology, Shenyang, China) and a middle-frequency magnetron sputtering (MS) system (5115D, Beiyu Vacuum Technology, Shenyang, China), respectively. For the AIP parameters, the arc current was 200 A, the bias voltage was −100 V, the N_2 flow rate was 30 mL/min, the O_2 flow rate was 30 mL/min, and the operation temperature was 180−200 °C. In comparison, the sputtering parameters were as follows: argon pressure 0.2 Pa, sputtering current 3.2 A, and substrate temperature 200 °C.

2.2 Isothermal and cyclic oxidation test

An isothermal oxidation test was performed in a muffle furnace in static air at 1050 °C for 200 h. Prior to the experiment, alumina crucibles were pre-heated at 1200 °C until no mass change was observed. A cyclic oxidation test was carried out in open air using an automated vertical furnace. Each cycle consisted of maintaining coated samples at 1050 °C for 1 h, followed by cooling them in air for 10 min. The mass change for both the isothermal and cyclic oxidation tests was obtained from three parallel samples using an electronic balance (BP211D, Sartorius, Germany) with an accuracy of 0.01 mg.

2.3 Characterization

The fractured sample was prepared by first cutting a slit with a wire cutting machine and then breaking it off. The morphology and chemical composition were characterized using a tungsten filament scanning electron microscopy (10 kV, TFSEM, JCM−7000 NeoScope, JEOL) equipped with an energy dispersive X-ray spectrometer (EDS). X-ray diffraction (XRD, PANalytical

Empyrean Series 2, Britain) with Cu K_α radiation (2θ range: 10°−90°, step size: 0.014°) was used for phase identification. The detailed grain microstructure was examined using a transmission electron microscope (TEM, JEM−2100 F, JEOL, Tokyo, Japan).

3 Results

3.1 Microstructure and composition of as-deposited coatings

Figure 1 shows the surface morphologies of the AIP NiCrAlY coating after annealing. It can be observed that the AIP NiCrAlY coating became homogeneous with dark particles scattering in a relatively light base after vacuum annealing. This typical microstructure is often considered as β-NiAl in γ/γ' matrix, as reported in Refs. [19−24], which might be due to the precipitation of the β phase from an oversaturated γ' phase during the preparation processes.

Figure 2 shows the surface and fractured sectional morphologies of the as-deposited MS nanocrystalline coating. The surface morphologies in Figs. 2(a) and (b) show randomly dispersed bulges and a detailed cluster composed of abundant irregular granules. Simultaneously, fractured sections cut by wire electrical discharge machining (WEDM) exhibited a typical columnar microstructure with a thickness of 30 μm. The coating/substrate interface was successfully chemically bonded after vacuum annealing (see Figs. 2(c, d)).

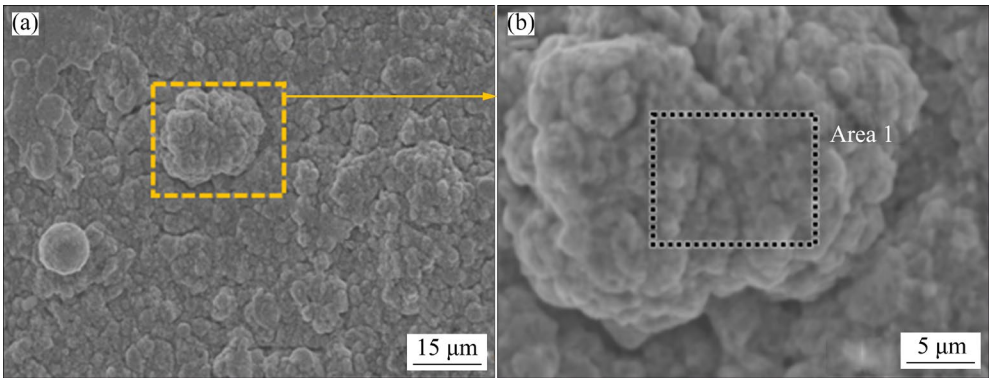

Fig. 1 Surface morphologies of as-deposited AIP NiCrAlY coating

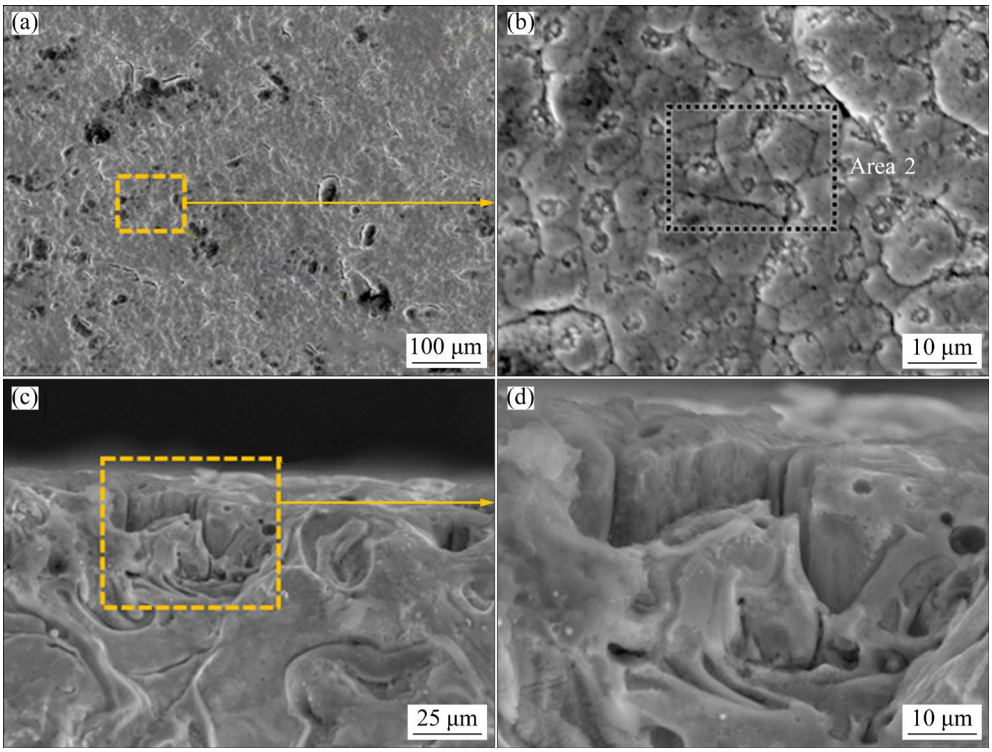

Fig. 2 Surface (a, b) and fractured sectional (c, d) morphologies of as-deposited MS NiCrAlY coating

The composition of the two coatings were detected by EDS and listed in Table 1. The selected areas (Area 1 in Fig. 1(b) and Area 2 in Fig. 2(b)) proved that the element compositions were basically in accordance with the target material.

Table 1 EDS results from different areas in Figs. 1 and 2 (wt.%)

Area	Ni	Cr	Al	Y
1	64.4	25.0	10.0	0.6
2	64.5	25.1	9.9	0.5

Figure 3 shows the XRD patterns of AIP and MS NiCrAlY coatings. It can be seen that both types of coatings are composed of β, γ/γ' and tiny α-Cr peaks, indicating that NiCrAlY coatings prepared by various methods (MS and AIP) both exhibit the same phase constitution.

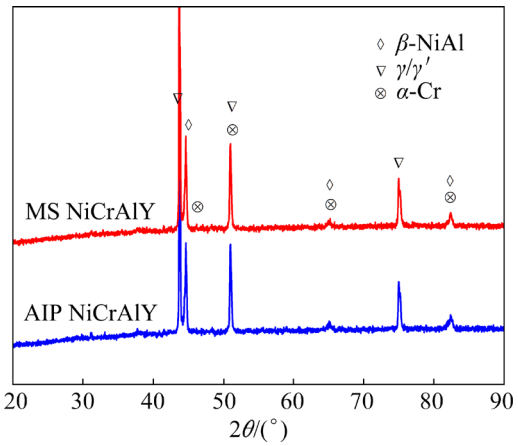

Fig. 3 XRD patterns of AIP and MS NiCrAlY coatings

3.2 Isothermal oxidation behavior

The mass gain and the square of mass gain for AIP and MS NiCrAlY coatings during the isothermal oxidation test at 1050 °C are shown in Figs. 4(a) and (b), respectively. The MS NiCrAlY exhibited a comparatively lower mass gain than AIP NiCrAlY during the stable oxidation stage (30−200 h), and its final total mass gain was 0.313 mg/cm^2, while that of the AIP NiCrAlY coating was 0.693 mg/cm^2. The squares of mass gain for the AIP and MS NiCrAlY coatings shown in Fig. 4(b) were calculated from experimental data of Fig. 4(a)). To avoid the disturbance of the initial volatile oxidation stage, the data at the stable oxidation stage were selected for linear fitting to obtain the oxidation rate constant K_p. The calculated K_p values for AIP and MS NiCrAlY were 9.88×10^{-4} and 4.41×10^{-4} mg^2/(cm^4·h), respectively. The MS NiCrAlY exhibited a lower oxidation rate than the AIP one.

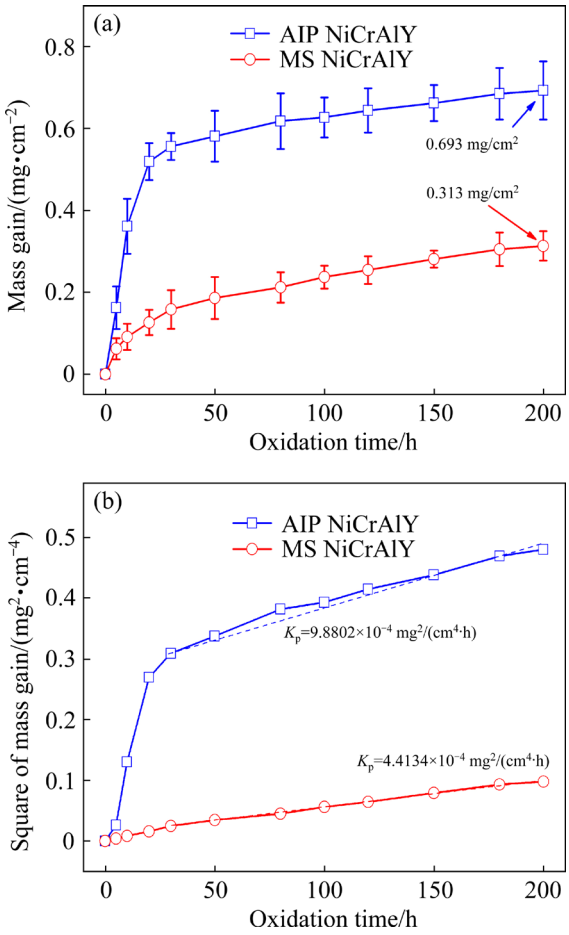

Fig. 4 Mass gain (a) and square of mass gain (b) curves of AIP and MS NiCrAlY coatings with oxidation time at 1050 °C

Figure 5 shows the surface morphologies of AIP and MS NiCrAlY coatings after the isothermal oxidation test for 200 h. As seen in Figs. 5(a) and (b), the oxide scale formed on the AIP NiCrAlY coating exhibited a typical discontinuous bulge, and the high-magnification image revealed a raised cauliflower shape. The EDS analysis implied that it is (Ni,Cr)Al_2O_4 spinel. Comparatively, the oxide scale formed on MS NiCrAlY was complete, continuous and dense, without obvious cracks and spalling. The corresponding EDS analysis (Table 2) indicates that it is composed of Al_2O_3.

Figure 6 shows the X-ray diffraction patterns of both two NiCrAlY coatings after isothermal oxidation at 1050 °C for 200 h. Based on the intensity of the diffraction peaks, it can be speculated

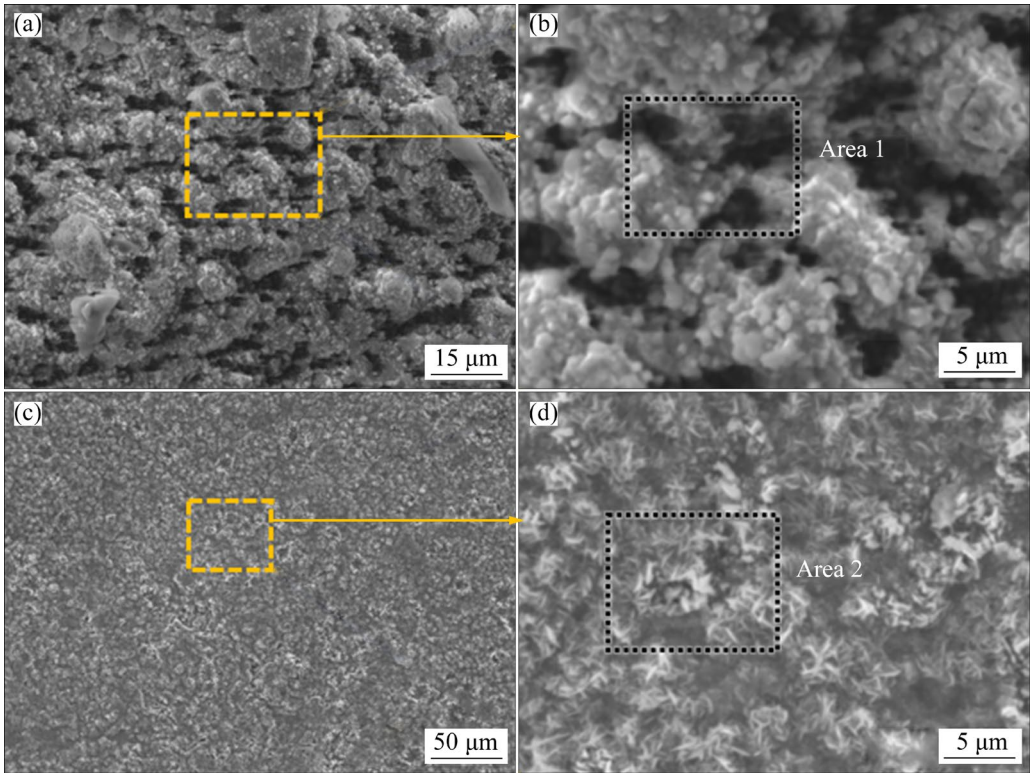

Fig. 5 Surface morphologies of AIP (a, b) and MS (c, d) NiCrAlY coatings after isothermal oxidation for 200 h

Table 2 EDS results of different areas in Fig. 5 (at.%)

Area	Ni	Cr	Al	Y	O
1	12.5	11.9	24.6	0.1	50.9
2	2.4	2.6	42.7	0.2	52.1

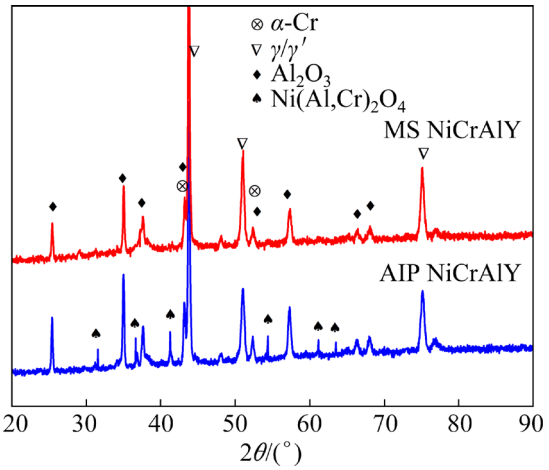

Fig. 6 XRD patterns of AIP and MS NiCrAlY coatings after isothermal oxidation for 200 h

that the formation of $Ni(Al,Cr)_2O_4$ on the MS NiCrAlY remains relatively inconspicuous, suggesting that its degradation degree is less severe than that of the AIP NiCrAlY coating.

3.3 Cyclic oxidation behavior

Figure 7 shows the mass change curves of both AIP and MS NiCrAlY coatings during cyclic oxidation test at 1050 °C. The AIP NiCrAlY coating exhibited a rapid mass increase during the initial oxidation stage, reaching up to 30 cycles, and then gradually stabilized until 150 cycles, at which its maximum value was 0.695 mg/cm^2. Subsequently, mass loss occurred at 180 and 200 cycles, suggesting that the oxide scale formed on the AIP NiCrAlY coating underwent noticeable peeling

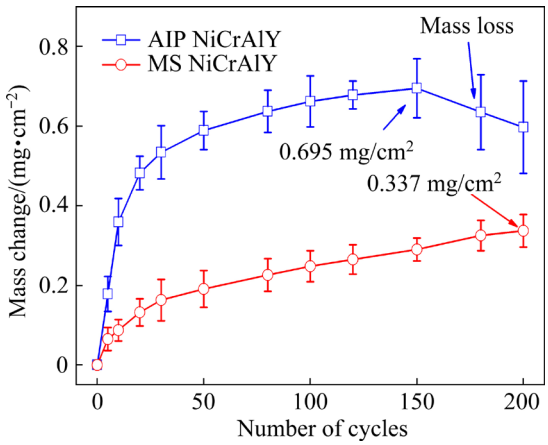

Fig. 7 Mass change curves of AIP and MS NiCrAlY coatings after cyclic oxidation at 1050 °C

after cyclic oxidation for 180 cycles. Conversely, the MS NiCrAlY coating did not experience any significant mass loss throughout the entire thermal cycling test, and the range of error fluctuations was narrow, which indicates that the oxide scale formed on the MS NiCrAlY coating exhibits excellent spalling resistance during cyclic oxidation test.

Figure 8 shows the surface morphologies of AIP and MS NiCrAlY coatings after cyclic oxidation for 200 cycles. The surface morphologies of the two NiCrAlY coatings exhibited distinct characteristics. The MS NiCrAlY coating exhibited a significant number of unevenly distributed protrusions, along with numerous cracks and scale spallation. A further high-magnification image revealed cauliflower-like and sharp protrusions accompanied by a sheet-like broken oxide scale. In contrast, the oxide scale formed on the MS nanocrystalline NiCrAlY coating was dense and complete with no visible cracks or spalling pits. These results effectively confirmed that the nanocrystalline NiCrAlY exhibited superior oxide scale adhesion and spallation resistance during the thermal cycling test. The EDS results shown in Table 3 verified that the oxide scale formed on the MS NiCrAlY coating was primarily composed of Al_2O_3.

Figure 9 shows the cross-sectional morphologies and corresponding elemental distributions of AIP NiCrAlY coatings after cyclic oxidation for 200 h. As can be observed from Fig. 9(a), the discontinuous black oxide at the bottom and the loose, porous, light-colored spinel at the top were distributed throughout the TC/BC interface. Further analysis of the elemental distributions confirmed that the spinel oxide was composed of Ni, Cr, Al and O, while the black oxide primarily consisted of Al and O, which indicated that both Al_2O_3 and $Ni(Cr,Al)_2O_4$ formed simultaneously. Additionally, a distinct Cr-rich zone was visible at the bottom of the TGO due to the excessive consumption of aluminum, suggesting that significant coating degradation occurred in the AIP NiCrAlY coating.

Compared with the AIP coating, the cross-sectional morphology and corresponding elemental distributions of the MS NiCrAlY coating are presented in Fig. 10. The relevant results confirmed that a continuous, dense and exclusive Al_2O_3 scale firmly attached to the coating accompanied with numerous embedded oxide pegs.

Figure 11 shows the X-ray diffraction patterns of the two coatings after cyclic oxidation for 200 cycles. The results showed that the oxide scale of the nanocrystalline NiCrAlY coating consists exclusively of Al_2O_3.The degradation of the MS

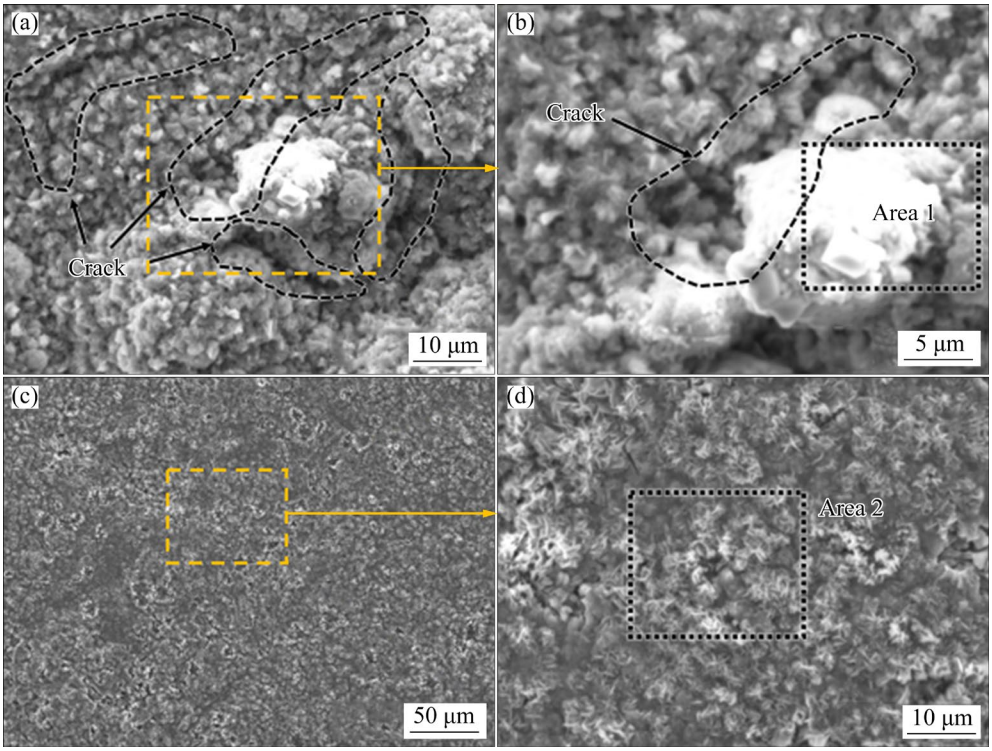

Fig. 8 Surface morphologies of AIP (a, b) and MS (c, d) NiCrAlY coatings after cyclic oxidation for 200 cycles

Table 3 EDS results in different areas in Fig. 8 (at.%)

Area	Ni	Cr	Al	Y	O
1	11.9	12.6	23.7	0.2	51.6
2	2.1	2.1	41.8	0.2	53.8

NiCrAlY was slower, thus inhibiting the formation of the detrimental $Ni(Al,Cr)_2O_4$ spinel phase.

4 Discussion

4.1 Effect of nanocrystalline on oxidation rate

The maintenance of a continuous, dense and exclusive α-Al_2O_3 scale can offer excellent oxidation resistance under high temperature exposure. To achieve a continuous α-Al_2O_3 scale, the Al content within the coating interior must reach a critical value. The critical value ($N_{Al}^{(1)}$) is expressed as follows [24−28]:

$$N_{Al}^{(1)} > \left[\frac{\pi g}{2}\frac{N_o D_o V_m}{D_{Al} V_{ox}}\right]^{1/2} \quad (1)$$

where N_oD_o is the oxygen permeability; D_{Al} is the diffusion coefficient of Al; g is a factor decided by volume fraction oxide required for transition from internal to external oxide; V_m and V_{ox} are the molar volumes of alloy and oxide, respectively.

To determine the grain size of the MS NiCrAlY coating, a TEM image and corresponding grain size distribution are shown in Fig. 12. The grain size of the MS coating varies between 15 and 60 nm, with an average grain size of (29.21±1.99) nm. Additionally, a significant number of high-density dislocations are distributed within some grains. In contrast, the grain size of the AIP NiCrAlY typically ranges in 700−1600 nm [25−30].

The nanocrystalline NiCrAlY coating with abundant grain boundaries facilitates the diffusion of Al element, significantly enhancing the diffusion coefficient of Al (D_{Al}). This reduction in the critical value required for the formation of protective α-Al_2O_3 makes it easier to achieve a continuous and dense Al_2O_3 scale. In contrast, conventional NiCrAlY coatings are more prone to forming loose

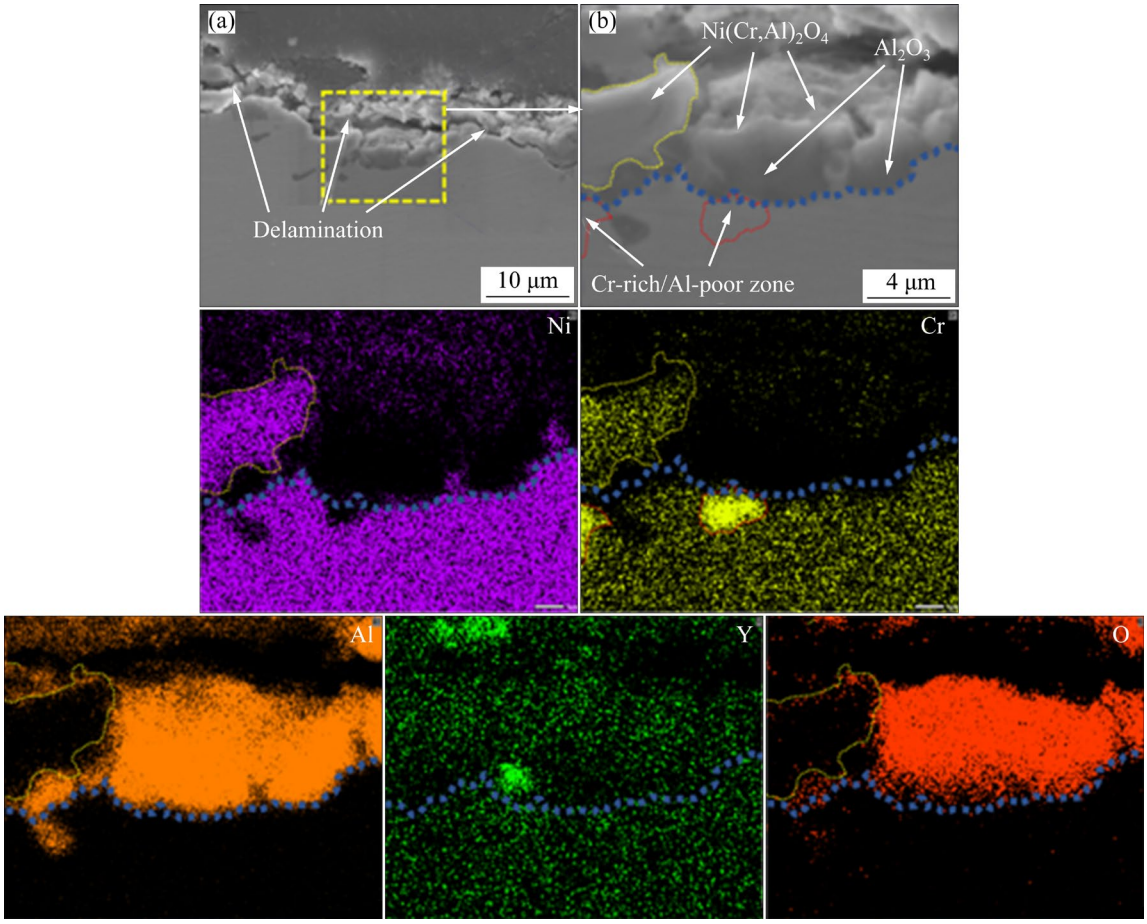

Fig. 9 Cross-sectional morphology and corresponding elemental distributions of AIP NiCrAlY coating after cyclic oxidation for 200 h

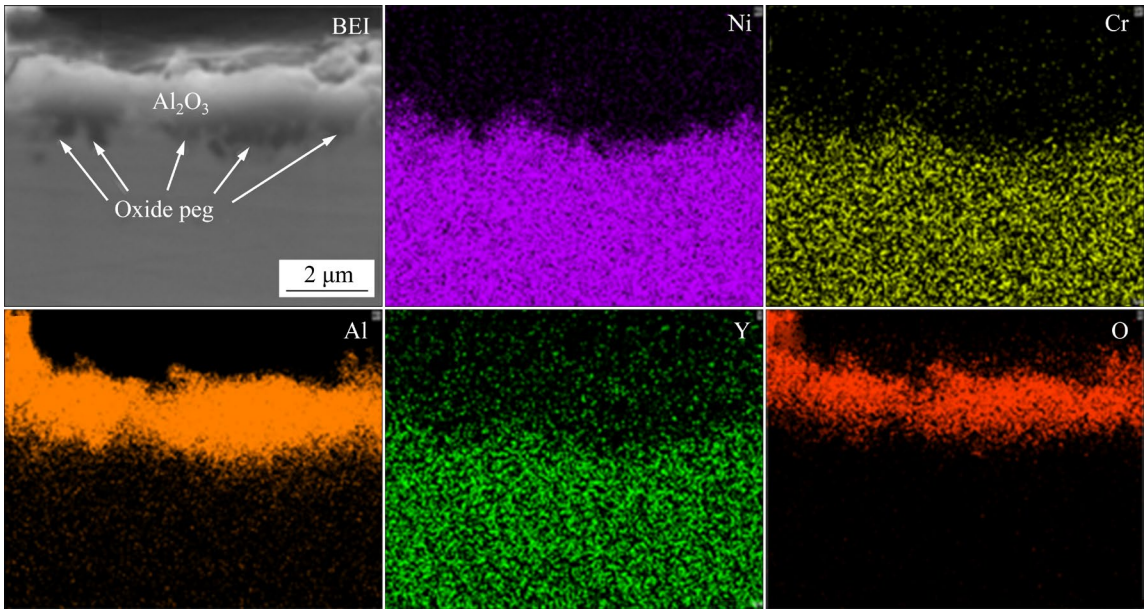

Fig. 10 Cross-sectional morphology and corresponding elemental distributions of MS NiCrAlY coating after cyclic oxidation for 200 h

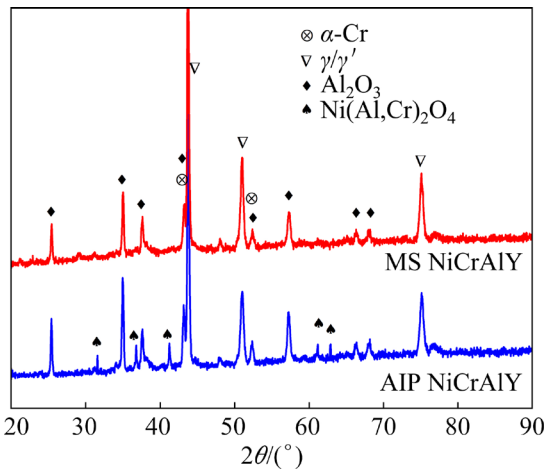

Fig. 11 XRD patterns of AIP and MS NiCrAlY coatings after cyclic oxidation for 200 h

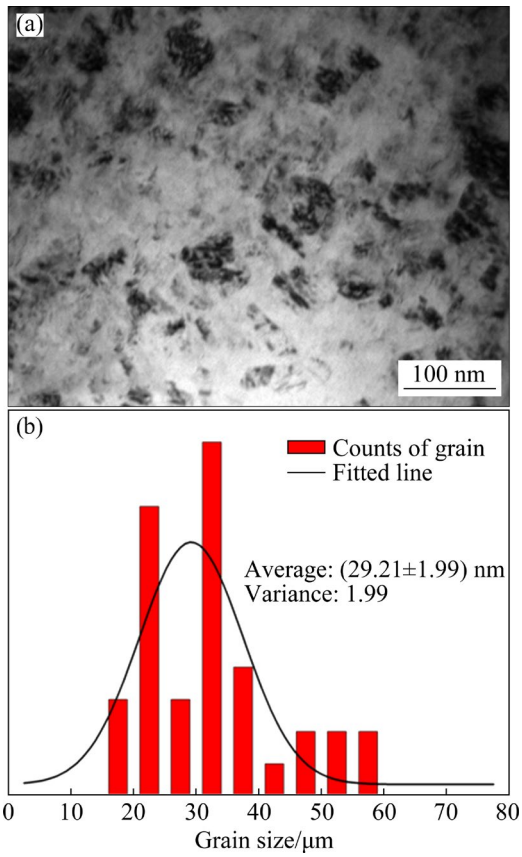

Fig. 12 TEM image (a) and corresponding grain size distribution (b) of MS NiCrAlY nanocrystalline coating

and porous structural spinel oxide, as seen in Fig. 13. The earlier formation of a protective α-Al_2O_3 scale on the nanocrystalline NiCrAlY effectively reduces the oxygen partial pressure. Subsequently, the critical Al content required to form a continuous, dense α-Al_2O_3 scale [31−34]. Conversely, the weak protective $Ni(Cr,Al)_2O_4$ spinel formed on conventional NiCrAlY in the early stage can lead a vicious cycle of "spinel formation−excessive degradation−spinel formation" [35−38]. Furthermore, the abundant grain boundaries of the MS nanocrystalline NiCrAlY coating provide more nucleation sites for the oxide scale, allowing initial nucleation particles to grow and connect with each other, resulting in the formation of a fine-grained oxide scale [35,38,39].

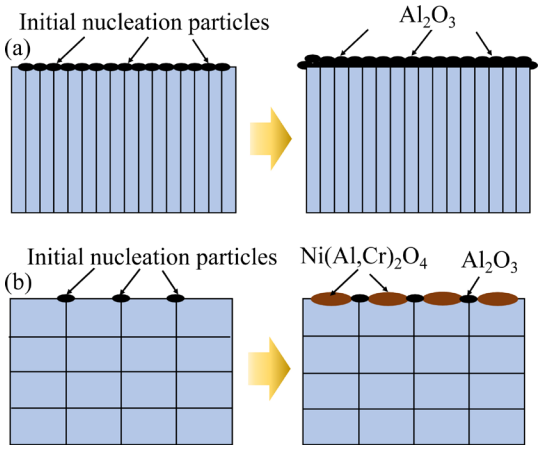

Fig. 13 Schematic diagram illustrating nucleation and growth of oxide scale on MS (a) and AIP (b) NiCrAlY coatings

According to the classic oxidation theory, the growth rate of TGO is mainly determined by the outward diffusion of Al and the inward diffusion of O. The decisive factor hindering the diffusion rate is the barrier effect of the early-formed oxide. The final mass gain of nanocrystalline NiCrAlY coatings after isothermal exposure at 1050 °C for 200 h is 54.8% less than that of conventional NiCrAlY. Additionally, the oxidation rate constant (K_p) is notably decreased by 55.3%, suggesting that nanocrystalline evidently plays a positive role in reducing the oxidation rate.

4.2 Effect of nanocrystalline on scale adhesion

It is generally believed that the dense alumina has better spallation resistance than spinel oxide. Therefore, we believe that the nanocrystalline NiCrAlY coating can enhance the spalling resistance of the oxide scale by suppressing the formation of the harmful spinel phase ($Ni(Cr,Al)_2O_4$). Furthermore, the scale adhesion is also directly associated with the internal stress level.

Usually, internal stress generated in the oxide scale is mainly due to the oxide growth and the mismatch in the coefficient of thermal expansion (CTE) between the scale and the coating during thermal cycling. There are three main mechanisms for releasing this internal stress [35,38]: (1) Plastic deformation of the oxide scale; (2) Plastic deformation at the scale/coating interface; (3) Cracking or peeling of the oxide scale. The plastic deformation of the oxide scale at elevated temperature is mainly caused by diffusion creep. The creep rate ($\dot{\varepsilon}$) is closely related to the grain size [35,38]:

$$\dot{\varepsilon}=\frac{\sigma\Omega}{d^2KT}\left(B_1D_v+\frac{B_2\delta D_b}{d}\right) \tag{2}$$

where B_1 and B_2 are constants, σ is the stress, Ω is the atomic volume, D_v and D_b are intragranular diffusion coefficient and grain boundary diffusion coefficient, respectively, δ is the grain width, K is the Boltzmann constant, T is the thermodynamic temperature, and d is the grain size. When grain boundary diffusion dominates, Eq. (2) can be simplified as [35,38]

$$\dot{\varepsilon}=\frac{\delta\sigma\Omega BD_b}{d^3KT} \tag{3}$$

Equation (3) indicates that the creep rate is inversely proportional to the third power of the grain size, which means that the finer the oxide scale grain, the more beneficial it is for creep deformation [35,38]. The MS nanocrystalline NiCrAlY coating has finer oxide scale grain than conventional NiCrAlY, making it easier to release internal stress through plastic deformation [35,36]. Additionally, the embedded oxide pegs formed on the nanocrystalline NiCrAlY further enhance the adhesion of the oxide scale (see Fig. 10). Therefore, its oxide scale has better anti-stripping performance during reciprocating heating and cooling cycle (see Fig. 8). In contrast, the conventional NiCrAlY coating generates a coarse, messy and fragile spinel, which worsens the oxide adhesion during thermal cycling [34,35−39].

The unique columnar crystal structure of the MS coating can provide channels for the rapid outward diffusion of Al, greatly facilitating the selective oxidation of Al. In addition, the high density of nanoscale grain boundaries provides a vast number of nucleation sites for α-Al_2O_3, promoting the formation of a dense distribution of oxide islands on the surface. Over a short period, these oxide islands coalesce and connect, forming a continuous and dense protective oxide scale dominated by α-Al_2O_3. In contrast, the AIP coating, with its coarser equiaxed crystalline microstructures, exacerbates the difficulty of outward diffusion. During the earliest oxidation stage, when the multicomponent NiCoCrAlY coating is fully exposed to a high-temperature atmosphere, all

components of the coating have a potential to participate in the oxidation process. The micron-sized grain boundaries of the AIP coating lead to a discrete distribution of the oxide islands nucleated on the surface. These oxide islands are primarily composed of θ-Al_2O_3 and α-Al_2O_3. When local microstructural defects in the coating result in an insufficient supply of Al, it becomes challenging to sustain the exclusive growth of the alumina scale Ni and Cr diffuse toward the outer surface through the vacancies left by Al, leading to the formation of $NiCr_2O_4$ spinel. As the oxidation continues, the inherently faster growth rate of transient oxides, such as θ-Al_2O_3 and $NiCr_2O_4$ spinel, causes rapid thickening of TGO. Notably, the severe surface undulation of the AIP coating is accompanied by frequent voids and cracks within the oxide scale, which are mainly due to the volume shrinkage generated by the phase transformation.

5 Conclusions

(1) The nanocrystalline NiCrAlY coating exhibits superior isothermal and cyclic oxidation resistance compared with the conventional NiCrAlY at 1323 K.

(2) The mass gain and parabolic rate constant K_p of the nanocrystalline NiCrAlY coating are 45.2% and 44.7% lower than those of the conventional NiCrAlY coating.

(3) During cyclic oxidation, the spallation tendency of the oxide scale is evidently decreased by nanocrystallization, due to the formation of a continuous, compact, adherent, and slow-growing exclusive α-Al_2O_3 scale.

CRediT authorship contribution statement

Chun-tang YU: Methodology, Formal analysis, Writing − Original draft; **Shu-tao CHEN** and **Xiao-yun LI:** Experiment participator, Data curation; **Wen-yao SUN:** Experiment participator, Review, Editing; **Min FENG:** Data curation, Experiment participator, Review, Editing; **Cheng-yang JIANG:** Experiment participator, Editing; **Wan-qi PU** and **Han-qing XIE:** Experiment participator, Data curation; **De-quan WU:** Experiment participator; **Sheng-long ZHU** and **Fu-hui WANG:** Supervision.

Declaration of competing interest

The authors declare that they have no known competing financial interests or personal relationships that could have appeared to influence the work reported in this paper.

Acknowledgments

This work was financially supported by the National Natural Science Foundation of China (No. 52101075), China Postdoctoral Science Foundation (Nos. 2021M700557, 2022M723272), Postdoctoral Science Foundation Project of Chongqing Natural Science Foundation (Nos. cstc2021jcyj-bshX0053, cstc2021jcyj-bshX0039), and Scientific Research Foundation of Chongqing University of Technology (No. 2020ZDZ004).

References

[1] EVANS A G, MUMM D R, HUTCHINSON J W, MEIER G H, PETTIT F S. Mechanisms controlling the durability of thermal barrier coatings [J]. Progress in Materials Science, 2001, 46: 505−553.

[2] PADTURE N P, GELL M, JORDAN E H. Thermal barrier coatings for gas-turbine engine applications [J]. Science, 2002, 296: 280−284.

[3] WANG Jin-long, CHEN Ming-hui, YANG Lan-lan, SUN Wen-yao, ZHU Sheng-long, WANG Fu-hui. Nanocrystalline coatings on superalloys against high temperature oxidation: A review [J]. Corrosion Communications, 2021, 1: 58−69.

[4] YU Chun-tang, LIU He, JIANG Cheng-yang, BAO Ze-bin, ZHU Sheng-long, WANG Fu-hui. Modification of NiCoCrAlY with Pt: Part II. Application in TBC with pure metastable tetragonal (t') phase YSZ and thermal cycling behavior [J]. Journal of Materials Science and Technology, 2019, 35: 350−359.

[5] SONG Shan-guang, TAN Shi-lei, QI Xiao-xiao, WANG Wei, WANG Li-li. Effect of ball peening of substrate on microstructure, phase evolution and properties of electrophoretically deposited YSZ/(Ni,Al) composite coatings [J]. Transactions of Nonferrous Metals Society of China, 2016, 26: 2966−2975.

[6] YU Chun-tang, LIU He, ZHANG Jia, ULLAH A, BAO Ze-bin, JIANG Cheng-yang, ZHU Sheng-long, WANG Fu-hui. Gradient thermal cycling behavior of a thermal barrier coating system constituted by NiCoCrAlY bond coat and pure metastable tetragonal nano-4YSZ top coat [J]. Ceramics International, 2019, 45: 15281−15289.

[7] WANG Wen-chang, LI Jia-xing, GE Yuan, KONG De-jun. Structural characteristics and high-temperature tribological behaviors of laser cladded NiCoCrAlY−B_4C composite coatings on Ti6Al4V alloy [J]. Transactions of Nonferrous Metals of Society of China, 2021, 31: 2729−2739.

[8] XIE Yu-jiang, WANG De, WANG Ming-sheng, YE Wei. Evaluation of three kinds of MCrAlY coatings produced by electrospark deposition [J]. Transactions of Nonferrous Metals of Society of China, 2016, 26: 1647−1654.

[9] SEO D, OGAWA K, SUZUKI Y, ICHIMURA K, SHOJI T, MURATA S. Comparative study on oxidation behavior of

selected MCrAlY coatings by elemental concentration profile analysis [J]. Applied Surface Science, 2008, 255: 2581−2590.

[10] YU Chun-tang, XIE Han-qing, LI Shuai, JIANG Cheng-yang, BAO Ze-bin, ZHANG Wei, ZHANG Lei, PU Wan-qi, ZHU Sheng-long, WANG Fu-hui. Thermal cycling and interface bonding performance of single phase (Ni,Pt)Al coating with and without pure metastable tetragonal phase 4YSZ [J]. Applied Surface Science, 2023, 615: 156326.

[11] YU Chun-tang, PU Wan-qi, LI Shuai, BAO Ze-bin, CHENG Ren-ju, JIANG Cheng-yang, LIU Zheng-liang, ZHANG Wei, ZHANG Lei, ZHAO Sui-bo, XIE Han-qing, ZHU Sheng-long, WANG Fu-hui. High-temperature performance of Pt-modified Ni−20Co−28Cr−10Al−0.5Y coating: Formation mechanism of Pt-rich overlayer and its effect on thermally grown oxide failure [J]. Surface and Coatings Technology, 2023, 461: 129422.

[12] YU Chun-tang, JIANG Yi-ming, LI Shuai, BAO Ze-bin, JIANG Cheng-yang, WANG Jie-min, PU Wan-qi, XIE Han-qing, ZHANG Lei, ZHANG Wei, ZHU Sheng-long, WANG Fu-hui. Effect of Hf addition on initial microstructure of (Ni,Pt)Al coating and inhibiting the detrimental sulfur during high temperature exposure at 1150 °C [J]. Corrosion Science, 2023, 221: 111375.

[13] GAO Jun-guo, TANG Zhi-hui, WANG Chang-liang, GUO Meng-qiu, CUI Yong-jing. Microstructure, mechanical and oxidation characteristics of detonation gun and HVOF sprayed MCrAlYX coatings [J]. Transactions of Nonferrous Metals of Society of China, 2015, 25: 817−823.

[14] HAN Yu-jun, ZHU Zhi-ying, LI Xiao-quan, SHEN Sai-gang, YE Fu-xing. Effects of vacuum pre-oxidation process on thermally-grown oxides layer of CoCrAlY high temperature corrosion resistance coating [J]. Transactions of Nonferrous Metals of Society of China, 2015, 25: 3305−3314.

[15] ZHANG Xiao-feng, ZHOU Ke-song, DONG Shu-juan, XU Wei, SONG Jin-bing, LIU Min. Effect of Al-deposition on erosion resistance of plasma sprayed thermal barrier coating [J]. Transactions of Nonferrous Metals of Society of China, 2015, 25: 2587−2593.

[16] CHEN Ming-hui, ZHU Sheng-long, WANG Fu-hui. High temperature oxidation of NiCrAlY, nanocrystalline and enamel-metal nano-composite coatings under thermal shock [J]. Corrosion Science, 2015, 100: 556−565.

[17] YANG Lan-lan, CHEN Ming-hui, WANG Jin-long, ZHU Sheng-long, WANG Fu-hui. A duplex nanocrystalline coating for high-temperature applications on single-crystal superalloy [J]. Corrosion Science, 2016, 102: 72−83.

[18] WANG Jin-long, CHEN Ming-hui, YANG Lan-lan, LIU Li, ZHU Sheng-long, WANG Fu-hui, MENG Guo-ze. The effect of yttrium addition on oxidation of a sputtered nanocrystalline coating with moderate amount of tantalum in composition [J]. Applied Surface Science, 2016, 366: 245−253.

[19] YANG Ying-fei, YAO Hong-rui, BAO Ze-bin, REN Pan, LI Wei. Modification of NiCoCrAlY with Pt: Part I. Effect of Pt depositing location and cyclic oxidation performance [J]. Journal of Materials Science and Technology, 2019, 35: 341−349.

[20] PENG Xin, JIANG Su-meng, GONG Jun, SUN Xu-dong, SUN Cao. Preparation and hot corrosion behavior of a NiCrAlY + AlNiY composite coating [J]. Journal of Materials Science and Technology, 2016, 32: 587−592.

[21] HOU Shao-jun, ZHU Sheng-long, WANG Fu-hui. A magnetron sputtered microcrystalline β-NiAl coating for SC superalloys: Part I. Characterization and comparison of isothermal oxidation behavior at 1100 °C with a NiCrAlY coating [J]. Applied Surface Science 2015, 324: 1−12.

[22] WANG Jia-hao, LI Dang-guo, SHAO Tian-min. Hot corrosion and electrochemical behavior of NiCrAlY, NiCoCrAlY and NiCoCrAlYTa coatings in molten NaCl−Na_2SO_4 at 800 °C [J]. Surface and Coatings Technology, 2022, 440: 128503.

[23] SHI Pei-ying, WANG Wen-zhen, WAN Shan-hong, GAO Qiang, SUN Hu-wei, FENG Xiao-chun, YI Ge-wen, XIE Er-qing, WANG Qi-hua. Tribological performance and high temperature oxidation behaviour of thermal sprayed Ni- and NiCrAlY-based composite coatings [J]. Surface and Coatings Technology, 2021, 405: 126615.

[24] TERNER M, LEE J, RUGGIERI B, COPIN E, OSTROVSKAYA O, BADINI C, LOURS P, HONG H U. Thermal shock resistance of a NiCrAlY-coated Alloy 625 system produced by laser powder bed fusion [J]. Surface and Coatings Technology, 2021, 417: 127217.

[25] TEXIER D, COPIN E, FLORES A, LEE J, TERNER M, HONG H U, LOURS P. High temperature oxidation of NiCrAlY coated Alloy 625 manufactured by selective laser melting [J]. Surface and Coatings Technology, 2020, 398: 126041.

[26] MOSKAL G, NIEMIEC D, CHMIELA B, KAŁAMARZ P, DUREJKO T, ZIĘTALA M, CZUJKO T. Microstructural characterization of laser-cladded NiCrAlY coatings on Inconel 625 Ni-based superalloy and 316L stainless steel [J]. Surface and Coatings Technology, 2020, 387: 125317.

[27] HE Jian-hong, Advanced MCrAlY alloys with doubled TBC lifetime [J]. Surface and Coatings Technology, 2022, 448: 128931.

[28] TOLPYGO V K, DRYDEN J R, CLARKE D R. Determination of the growth stress and strain in α-Al_2O_3 scales during the oxidation of Fe−22Cr−4.8Al−0.3Y alloy [J]. Acta Materialia 1998, 46: 927−937.

[29] YU Chun-tang, LIU He, ULLAH A, BAO Ze-bin, ZHU Sheng-long, WANG Fu-hui. High-temperature performance of (Ni, Pt)Al coatings on second-generation Ni-base single-crystal superalloy at 1100 °C: Effect of excess S impurities [J]. Corrosion Science, 2019, 159: 108115.

[30] SHI Long, XIN Li, WANG Xin-yue, WANG Xiao-lan, WEI Hua, ZHU Sheng-long, WANG Fu-hui. Influences of MCrAlY coatings on oxidation resistance of single crystal superalloy DD98M and their inter-diffusion behaviors [J]. Journal of Alloys and Compounds, 2015, 649: 515−530.

[31] WANG Jin-long, CHEN Ming-hui, YANG Lan-lan, ZHU Sheng-long, WANG Fu-hui. Comparative study of oxidation and interdiffusion behavior of AIP NiCrAlY and sputtered nanocrystalline coatings on a nickel-based single-crystal superalloy [J]. Corrosion Science, 2015, 98: 530−540.

[32] WANG Fu-hui. The effect of nanocrystallization on the selective oxidation and adhesion of Al_2O_3 scales [J]. Oxidation of Metals, 1997, 48: 215−224.

[33] AJDELSZTAJN L, PICAS J A, KIM G E, BASTIAN F L, SCHOENUNG J, PROVENZANO V. Oxidation behavior of HVOF sprayed nanocrystalline NiCrAlY powder [J]. Materials Science and Engineering: A, 2002, 338: 33−43.
[34] WANG Fu-hui, LOU Han-yi, ZHU Sheng-long, WU Wei-tao. The mechanism of scale adhesion on sputtered micro-crystallized CoCrAl films [J]. Oxidation of Metals, 1996, 45: 39−50.
[35] BIRKS N, MEIER G H, PETTIT F S. Introduction to the high-temperature oxidation of Metals [M]. Cambridge: Cambridge University Press, 2006: 111−115.
[36] GIL A, NAUMENKO D, VASSEN R, TOSCANO J, SUBANOVIC M, SINGHEISER L, QUADAKKERS W J. Y-rich oxide distribution in plasma sprayed MCrAlY-coatings studied by SEM with a cathodoluminescence detector and Raman spectroscopy [J]. Surface and Coatings Technology, 2009, 204: 531−538.
[37] WANG Wen, YU Ping, WANG Fu-hui, ZHU Sheng-long. The effect of yttrium addition on the isothermal oxidation behavior of sputtered K38 nanocrystalline coating at 1273 K in air [J]. Surface and Coatings Technology, 2007, 201: 7425−7431.
[38] JIA Yi-xuan, ZHU Sheng-long, LIU Zheng-liang, SHEN Ming-li, WANG Fu-hui. Oxidation mechanism of Ni+CrAlYNO nanocomposite coating enhanced by a NiCrAlY buffer layer [J]. Corrosion Science, 2021, 180: 109184.
[39] AN Guo-sheng, LI Wen-sheng, WANG Zhi-ping, FENG Li, CHENG Bo, ZHOU Lan, LI Zhi-yu, ZHANG Yi. High-temperature oxidation and TGO growth behaviors of laser-modified YAG/YSZ double-ceramic-layer TBC [J]. Transactions of Nonferrous Metals of Society of China, 2023, 33: 1178−1192.

AIP 沉积和磁控溅射 Ni−25Cr−10Al−0.5Y 涂层在 1323 K 下的等温和循环氧化行为

余春堂[1]，陈曙韬[1]，李小云[1]，孙文瑶[2]，丰 敏[3,4]，
蒋成洋[5]，蒲万祺[1]，谢翰卿[1]，吴德权[6]，朱圣龙[7]，王福会[8]

1. 重庆理工大学 材料科学与工程学院，重庆 401320；
2. 哈尔滨工程大学 烟台研究院，烟台 264000；
3. 中国科学院大学 杭州高等研究院 化学与材料科学学院，杭州 310024；
4. 中国科学院 上海硅酸盐研究所 高性能陶瓷与超微结构国家重点实验室，上海 200050；
5. 北京航空航天大学 中法航空学院，杭州 310023；
6. 西南技术工程研究所，重庆 400039；
7. 中国科学院 金属研究所 师昌绪先进材料创新中心，沈阳 110016；
8. 东北大学(分部) 沈阳材料科学国家实验室，沈阳 110819

摘 要：采用多弧离子镀(AIP)和磁控溅射(MS)两种方法在 K417 高温合金表面制备 Ni−25Cr−10Al−0.5Y (NiCrAlY)涂层。在 1323 K 静态空气下对两种 NiCrAlY 涂层的等温和循环氧化行为进行评价。结果表明，在 1323 K 下，纳米晶 NiCrAlY 涂层比普通 NiCrAlY 涂层具有更好的等温和循环氧化性能。纳米晶 NiCrAlY 涂层的质量增加和抛物速率常数 K_p 分别比传统 NiCrAlY 涂层的低 45.2%和 44.7%。在循环氧化过程中，由于形成了连续、致密、黏附性强、生长缓慢的 α-Al_2O_3 氧化膜，纳米化使得氧化膜的剥落倾向明显降低。另外，讨论了纳米晶 NiCrAlY 涂层性能提升的机理。

关键词：MCrAlY；纳米晶；热生长氧化物；高温氧化；剥落

(Edited by Xiang-qun LI)